# Photophysics of carbon nanotubes in organic polymer-toluene dispersions: Emission and excitation satellites and relaxation pathways

Sergei Lebedkin,[1,*,†] Frank Hennrich,[1] Oliver Kiowski,[1,2] and Manfred M. Kappes[1,2,*,‡]
[1]*Forschungszentrum Karlsruhe, Institut für Nanotechnologie, 76021 Karlsruhe, Germany*
[2]*Universität Karlsruhe, Institut für Physikalische Chemie, 76128 Karlsruhe, Germany*
(Received 18 February 2008; published 29 April 2008)

We have prepared toluene-polymer dispersions of single-walled carbon nanotubes (SWNTs) containing only one or a few specific semiconducting $(n,m)$ species. These have large helical angles and manifest a high discrimination against larger-diameter SWNTs, metallic species, and nanotube aggregates. Such $(n,m)$-narrowed dispersions proved especially valuable for identification of low-intensity photoluminescence (PL) features as well as relaxation pathways, e.g., for the optically active $E_{22}$ and $E_{11}$ excitons, in specific nanotubes. Among other features, PL excitation and emission satellites at $\sim(E_{11}+95)$ and $\sim(E_{11}-200)$ meV, respectively, were resolved. We show that the $E_{22}$ exciton primarily decays ($\geq 80\%$) to the optical $E_{11}$ exciton. A minor decay pathway likely involves relaxation into "dark" deep excitonic states, which weakly emit at $\sim 40$ and $\sim 140$ meV below $E_{11}$. In addition, we report PL polarization measurements, supporting assignment of transverse $E_{12,21}$ photoexcitations, and PL quantum yields for $(n,m)$ nanotubes in toluene-polymer dispersions.

DOI: 10.1103/PhysRevB.77.165429 PACS number(s): 78.67.Ch, 78.55.−m, 81.07.De

## I. INTRODUCTION

Recently, Nish *et al.*[1] and Chen *et al.*[2] showed that single-walled carbon nanotubes (SWNTs) can be prepared as stable solutions of individual nanotubes in toluene by using a fluorene-based organic polymer as a dispersing and stabilizing agent. This observation is unprecedented insofar as SWNT dispersions in pure organic solvents, for instance, in *N*-methyl-pyrrolidone, tend to flocculate and contain only a minor fraction of individual nanotubes.[3] Moreover, toluene-polymer dispersions are in many respect superior to "standard" water-surfactant dispersions of SWNTs.[4] Compared to the latter, absorption and photoluminescence (PL) spectra of toluene-polymer dispersions indicate pronounced selectivity to semiconducting vs metallic nanotubes, selectivity to specific nanotube structures [defined by helicity indices $(n,m)$], sharper PL peaks, and an increased emission quantum yield of about 1%.[1,2] We will show below that applying ultracentrifugation to polymer-toluene dispersions can further narrow the $(n,m)$ distribution to only one or few well-separated $(n,m)$ species. The PL of such dispersions is relatively simple in that only a few major PL peaks are seen, associated with photoexcitation of the optically active ("bright") $E_{22}$ and $E_{11}$ excitonic states and radiative recombination of the $E_{11}$ state in semiconducting nanotubes.[5] The PL also reveals numerous low-intensity PL emission and photoluminescence excitation (PLE) satellite features (typically obscured by PL of other $(n,m)$ species in aqueous suspensions), thus providing further insight into the electronic (excitonic) structure and photophysics of SWNTs.

In this paper, we describe the PL and absorption spectra of $(n,m)$-narrowed dispersions of SWNTs in toluene-polymer. These data allow us to quantify the efficiency of $E_{22}\rightarrow E_{11}$ decay (a primary relaxation process for the $E_{22}$ state) and a PL quantum yield for dispersed $(n,m)$ species. A previously proposed (minor) relaxation pathway for the $E_{22}$ state via optically "dark" states,[6] down to deep dark states below $E_{11}$ (which show up as weak emission satellites),[7–9] is revisited on the basis of the improved spectral data. PL polarization measurements were also performed. These support an assignment of transverse $E_{12,21}$ photoexcitations, in accordance with the results of Miyauchi *et al.*[10] for SWNTs in an aqueous dispersion. Our data show that a characteristic "crossing" pattern in PL maps of samples comprising several $(n,m)$ species excited in the $E_{11}$ region—previously inferred to be a signature of energy transfer between nanotubes[11]—is, in fact, a superposition of PLE and emission satellites. These also include a PLE satellite at $\sim 95$ meV above $E_{11}$ and a *G*-phonon-coupled emission satellite at $\sim 200$ meV below $E_{11}$, which have not been described so far.

## II. EXPERIMENTS

SWNT materials produced by (i) high-pressure catalytic pyrolysis of carbon monoxide (HiPco, Carbon Nanotechnologies) and (ii) by pulsed laser vaporization (PLV) of nickel-cobalt-graphite targets in an argon atmosphere at 1000 °C were primarily used in this work.[12] Typically, approximately 1 mg of SWNTs were added to 10 ml toluene containing 0.1 wt % of poly[9,9-dioctylfluorenyl-2,7-diyl] (POF) (American Dye Source) and treated (debundled) for 10 h in a 55 kHz ultrasonic bath (Branson Ultrasonics). After sonication, a dispersion was centrifuged at 154.000 g for 2 h; the upper $\sim 1/3$ of the volume was collected and used for further experiments. A similar procedure was also applied to other SWNT materials such as CoMo-CVD (South West NanoTechnologies) prepared by chemical vapor deposition on a silica-supported cobalt-molybdenum catalyst and PLV nanotubes prepared at 1100 and 1200 °C. The above two samples were selected as yielding the narrowest distributions of only a few $(n,m)$ species—apparently, the initial $(n,m)$ compositions of HiPco and PLV (1000 °C) materials are particularly favorable for this dispersion method. Absorption and PL spectra (see below) evidenced a very good stability

 

of toluene-POF dispersions of SWNTs over at least several weeks.

Photoluminescence spectra were recorded on a Fourier transform infrared spectrometer (Bruker IFS66) equipped with a liquid-nitrogen-cooled Ge photodiode (sensitive in the range of $\lambda_{em} \sim 800-1700$ nm) and a monochromatized excitation light source with a 250 W halogen lamp.[13] PL maps such as that in Fig. 2 were acquired for ~3 h by scanning the excitation wavelength $\lambda_{exc}$ in 3 nm steps. The spectral resolution corresponded to ~12–4 nm (varying from $\lambda_{exc}=500$ nm to $\lambda_{exc}=1400$ nm) and 20 $cm^{-1}$ for excitation and detection channels, respectively. The PL intensity was corrected for the wavelength-dependent excitation intensity and spectrometer response (both in relative photon flux units).[13] The first correction is critical for evaluation of the $E_{22} \rightarrow E_{11}$ relaxation efficiency (Sec. III D). It was done using a thermopile (Dexter) as a detector and checked with calibrated Si and Ge photodiodes (Thorlabs). Polarization measurements were performed using the Glan–Thompson prisms as the excitation and emission polarizers. The polarization factor $P(\lambda_{exc},\lambda_{em})$ was calculated according to[14]

$$P = (PL_{HH}PL_{VV} - PL_{HV}PL_{VH})/(PL_{HH}PL_{VV} + PL_{HV}PL_{VH}) \quad (1)$$

from four PL maps measured with different combinations of vertical ($V$) and horizontal ($H$) polarizations of excitation (first letter) and emission (second letter) light. Luminescence anisotropy $r$ is related to $P$ as $r=2P/(3-P)$. The maximal values of $P$ for randomly oriented molecules are +0.5 and −0.33 for collinear and perpendicular absorption and emission transition moments, respectively.[14] The PL quantum efficiency $\varphi_{PL}$ of dispersed SWNTs was measured relative to the fluorescence of LDS-722 laser dye in methanol ($\varphi_{PL}=0.11\pm0.01$) on a Spex Fluorolog-3 spectrometer equipped with a Hamamatsu R5509 near-infared photomultiplier (sensitive up to ~1400 nm). Emission of LDS-722 was itself calibrated against that of Rhodamine-6G in methanol ($\varphi_{PL}$ is taken as 0.95).[15] All preparations and measurements were done at ambient temperature.

## III. RESULTS AND DISCUSSION

### A. ($n$,$m$)-narrowed dispersions of single-walled carbon nanotubes in toluene-poly[9,9-dioctylfluorenyl-2,7-diyl]

In agreement with the results of Nish *et al.*[1] and Chen *et al.*,[2] we obtained SWNT dispersions in toluene-POF with a significant enrichment in semiconducting nanotubes having a large helical angle $\alpha$ close to that of metallic ($n$,$n$) nanotubes ($\alpha=30°$). Moreover, we found that ultracentrifugation is very useful to further narrow the ($n$,$m$) distribution and to remove residual nanotube aggregates—similar to a preparation of water-surfactant dispersions of SWNTs.[4]

According to absorption spectra and PL maps shown in Figs. 1–3, a centrifuged dispersion of HiPco nanotubes in toluene-POF contains practically only five ($n$,$m$) species [(7,5), (7,6), (8,6), (8,7), and (9,7)], whereas that of PLV nanotubes is dominated by (9,7) species, with a minor contribution of (8,6) and (8,7) nanotubes. The ($n$,$m$) assignment

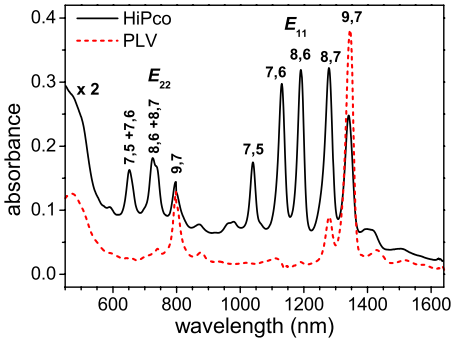


FIG. 1. (Color online) Absorption spectra of HiPco and PLV nanotubes sonicated in toluene-POF and left in the dispersion after ultracentrifugation. Optical path is 10 mm. The ($n$,$m$) assignment of $E_{11}$ and $E_{22}$ absorption peaks is supported by the PL data (see below). No background correction was applied to the spectra. The increase in absorption below ~550 nm is due to the POF polymer.

of $E_{11}$ and $E_{22}$ optical transitions follows that for the main PL peaks at $E_{22}$ excitation and $E_{11}$ emission energies for SWNTs in an aqueous dispersion,[16] taking into account a downshift of these energies in toluene-POF of about 15 and 20 meV, respectively, due to a different dielectric environment.[17] A low content of metallic nanotubes in the dispersions is evidenced by the absence of their peaks (blue-shifted relative to $E_{22}$ peaks of semiconducting nanotubes) and by an unusually low background in the absorption spectra.[1,2] The low absorption background is likely also due to the presence of only a small amount of residual nanotube aggregates. These are presumably responsible for broadened PL features and/or PL background typically observed for SWNTs in aqueous or organic dispersions.[3,4,8,11,13] Such broadening and PL background is nearly absent in Figs. 2 and 3.

To illustrate the effect of ultracentrifugation, Fig. S1 in Ref. 18 shows a PL map of PLV nanotubes sonicated in toluene-POF and stored overnight to allow big SWNT aggregates to precipitate. In addition to the dominant signal of (9,7) nanotubes as in Fig. 2, broad (overlapping) PL features are larger-diameter nanotubes are also observed. In the uncentrifuged dispersion, majority of the latter species likely comprise small aggregates of SWNTs. Apparently, the larger-diameter nanotubes cannot be well dispersed as individuals in toluene-POF (see also Refs. 1 and 2). This factor contributes to a narrow and sharp ($n$,$m$) distribution of SWNTs obtained after ultracentrifugation (Figs. 1–3). Such a sharp distribution is particularly helpful for analysis of weak PL emission and excitation satellites (Secs. III B and III C), which can be easily obscured by other ($n$,$m$) species, as well as for quantitative estimates of the relaxation processes in SWNTs (Sec. III D). The surprising selectivity of toluene-POF toward a small group of semiconducting SWNTs with a large helical angle can be explained by specific interactions between the POF molecules and SWNTs.[1] Details of these interactions, however, are not completely understood yet.

### B. Photoluminescence maps

As mentioned above, the main PL peaks indicated with ($n$,$m$) indices in Figs. 2(a) and 3 are related to $E_{22}$ excitation

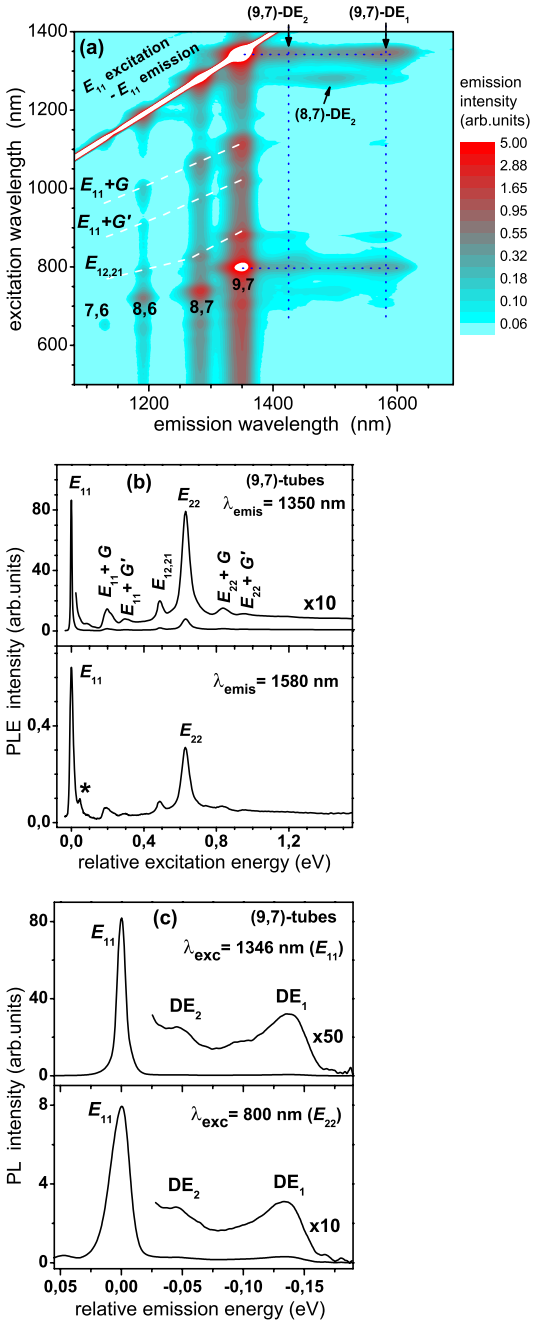


FIG. 2. (Color online) (a) PL map (emission intensity vs excitation and emission wavelength) of a $(n,m)$-narrowed dispersion of PLV nanotubes in toluene-POF. Emitting $(n,m)$ species are indicated at $E_{22}$-$E_{11}$ excitation-emission peaks. $E_{11}$-$E_{11}$ PL peaks are overlaid on the Rayleigh scattering line due to a very small Stokes shift. Dashed lines denote phonon-coupled $(E_{11}+G)$ and $(E_{11}+G')$ and transverse $E_{12,21}$ photoexcitations. Dotted lines show correlations between the major PL peaks and emission satellites $DE_1$ and $DE_2$ for (9,7) tubes (see text for details). Note that the PL intensity (color bar) is logarithmically scaled. (b) Photoluminescence excitation (PLE) spectra of (9,7) tubes at emission wavelengths of 1350 ($E_{11}$) and 1580 ($DE_1$). $G$- and $G'$-phonon-coupled PLE satellites are indicated for both $E_{11}$ and $E_{22}$ excitations. The asterisk indicates a contribution of the (8,7)-$DE_1$ satellite (see the PL map). (c) Emission spectra of (9,7) tubes at $E_{11}$ (1346 nm) and $E_{22}$ (800 nm) excitations.

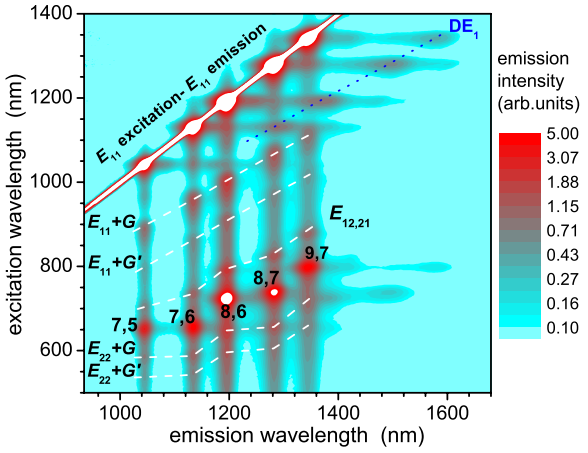


FIG. 3. (Color online) PL map of HiPco nanotubes dispersed in toluene-POF and comprising five emitting $(n,m)$ species with large helical angles. Notations of the PL peaks follow those in Fig. 2. The dotted line $DE_1$ indicates emission satellites $DE_1$ excited via $E_{11}$ transitions. These satellites are also clearly seen at $E_{22}$ excitations of (8,6), (8,7), and (9,7) nanotubes.

and $E_{11}$ emission of the corresponding optically active excitonic states in semiconducting SWNTs. Their emission linewidths of ~17–19 meV are notably smaller than ~25–30 meV reported for SWNTs in aqueous dispersions.[4,13] For comparison, emission linewidths of ~9–14 meV (under $E_{22}$ excitation) are typical for freely suspended SWNTs at ambient temperature.[17] Direct photoexcitation of the $E_{11}$ state of $(n,m)$ nanotubes followed by its radiative recombination generates $E_{11}$-$E_{11}$ PL peaks [Figs. 2(a) and 3]. They manifest a very small Stokes shift of less than ~2 meV and therefore overlap with the Rayleigh scattering line. A contribution of the scattered light to $E_{11}$-$E_{11}$ peaks of dominant $(n,m)$ species is, however, not very significant [for instance, ~10% of the total $E_{11}$ peak area in the PLE spectrum of (9,7) nanotubes in Fig. 2(b)]. This is due to an increased PL quantum yield of SWNTs in toluene-POF (see Sec. III E). In aqueous dispersions, the PL is weaker and broader and Rayleigh scattering usually hinders an accurate analysis of $E_{11}$-$E_{11}$ peaks and related satellite features.

We now turn to minor, i.e., low-intensity PL features. The dashed $(E_{11,22}-G,G')$ lines in Figs. 2 and 3 and Fig. S2 in Ref. 18 indicate phonon-coupled $E_{11,22}$ photoexcitations, whereas $G$ and $G'$ denote Raman-active normal and overtone vibrational modes in SWNTs.[19] These PLE satellites manifest substantial electron-phonon coupling in SWNTs. They are characteristic for the PL of ensembles of dispersed nanotubes as well as of individual substrate-deposited or freely-suspended nanotubes.[20–23] The dotted lines in Figs. 2 and 3 indicate $DE_2$ and $DE_1$ emission satellites. These features have already been observed for individual substrate-deposited nanotubes and SWNTs in aqueous dispersions and were attributed to weak emission from deep dark (or, more precisely, optically weakly allowed) excitonic states at ~40 and ~140 meV below $E_{11}$, respectively.[8,9] These states can be populated via $E_{11}$ or higher-energy photoexcitations, e.g., via decay of the latter to the $E_{11}$ state. Consequently, $DE_2$ and $DE_1$ emission satellites are expected to replicate at each

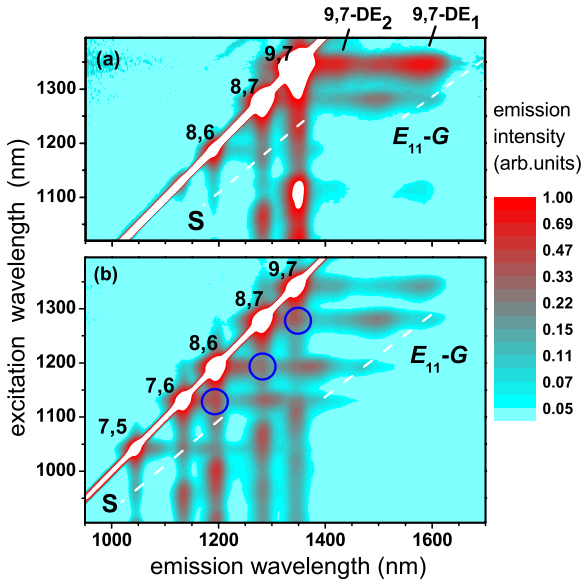


FIG. 4. (Color online) PL maps of (a) PLV and (b) HiPco nanotubes in the $E_{11}$ excitation region. Dashed lines ***S*** and $\boldsymbol{E_{11}}$**−*G*** indicate PL excitation and *G*-phonon-coupled emission satellites at $\sim(E_{11}+95)$ and $\sim(E_{11}-200)$ meV, respectively. A superposition of PLE and emission satellites in (b) produces a characteristic crossed stripes pattern, where some crossings are marked with open circles (see text).

photoexcitation on a PL map. However, this effect could not be conclusively observed in previous work because of very weak signals of individual nanotubes, broad PL features, and pronounced background in aqueous dispersions.[8,9] Figures 2(a) and 3 clearly show a replication pattern of the $DE_2$ and $DE_1$ satellites of (8,7) and (9,7) nanotubes. The vertical dotted lines highlight this pattern for the dominant (9,7) nanotubes. Note that this observation becomes possible because of the correspondingly low content of larger-diameter nanotubes (lower-energy emitters) in toluene-POF dispersions. Note further that the $DE_1$ satellites appear to be sensitive to different nanotube environments and/or perturbations: their intensity in aqueous dispersions amounts to ~0.1 of the amplitude of the main $E_{11}$-$E_{11}$ PL peaks,[9] whereas it is reduced to ~0.01 in toluene-POF (this work) and likely furthermore for suspended nanotubes.[9]

In addition to the PL satellites described above, SWNTs in toluene-POF demonstrate two further groups of PL satellites related to $E_{11}$ excitation, which have not been identified so far. In order to better illustrate these, the PL maps in the $E_{11}$ excitation region are separately shown in Fig. 4 and the satellites are indicated with dashed lines. The first group comprises very weak features appearing at the $E_{11}$ excitation and $\sim(E_{11}-200$ meV) emission energies for different $(n,m)$ species in both HiPco and PLV dispersions. We assign them to the *G*-phonon-coupled Stokes, i.e., $(E_{11}-G)$, emission satellites. As expected, the series of $(E_{11}-G)$ emission satellites lies collinear to stronger *G*-phonon-coupled $(E_{11}+G)$ excitation satellites (Fig. 4). The second group denoted with *S* includes PLE satellites at ~95 meV above $E_{11}$. They are clearly observed for (9,7) and (8,7) nanotubes in Fig. 4(a) and (7,5) and (7,6) nanotubes in Fig. 4(b). For other $(n,m)$ species in the second map, these features are hidden below $DE_{1,2}$ emission satellites of neighboring $(n,m)$ emitters. The origin of the *S* satellite is unclear. It might be due to photoexcitation of a dark (optically weakly allowed) excitonic state at $\sim(E_{11}+95)$ meV followed by relaxation and emission from the $E_{11}$ state. It might also be due to a phonon-coupled $E_{11}$ excitation involving non-Raman-active phonon(s). We note in this context that a high density of phonon states at ~85–100 meV has been calculated for SWNTs.[19]

The PL features discussed above are related to optical $E_{ii}$, $i=1,2,\ldots$, excitations that are polarized parallel to the SWNT axis. In the one-electron-excitation approximation, these axial excitations correspond to interband transitions between symmetric (*ii*) pairs of the van Hove singularities in the valence and conductance bands of SWNTs.[19] Cross-interband degenerate $E_{12}$ and $E_{21}$ photoexcitations are allowed for light polarized perpendicular to the SWNT axis. Despite a low cross section predicted for such transverse photoexcitations,[19] Miyauchi *et al.*[10] recently identified the corresponding PL peaks for SWNTs in a water-surfactant dispersion. Analogous PL peaks corresponding to $E_{12,21}$ excitation and $E_{11}$ emission are also clearly observed for SWNTs in toluene-POF (Figs. 2 and 3). The $E_{12,21}$-$E_{11}$ peaks show an ~140–200 meV downshift and only approximately ten times lower intensities relative to the main $E_{22}$-$E_{11}$ peaks—similar to results for SWNTs in a water-surfactant dispersion.[10] The assignment of $E_{12,21}$ photoexcitations was also proven by PL polarization measurements (Sec. III C). The energies and assignments of these and other PL peaks observed for $(n,m)$ nanotubes in toluene-POF are listed in Table S1 in Ref. 18.

A concluding remark in Sec. III B concerns a characteristic "crossed stripes" pattern below the $E_{11}$-$E_{11}$ line, which is generated by partly overlapping PLE and emission satellites of several neighboring $(n,m)$ emitters in Fig. 4(b). The graphical appearance of this pattern depends somewhat on the false color intensity scale used in the PL map. However, the crossing points [some of them are marked with open circles in Fig. 4(b)] always appear as a result of signal summation and/or accidentally proximal satellites. Such crossings might be erroneously considered as "independent" PL features. Recently, Tan *et al.*[11] ascribed a similar PL pattern observed for SWNTs in a water-surfactant dispersion to electronic (excitonic) energy transfer (EET) between $(n,m)$ species in nanotube aggregates (bundles). In their interpretation, the upper marked crossing in Fig. 4(b) would, for instance, correspond to photoexcitation of (8,7) nanotubes in some SWNT aggregates containing also (9,7) nanotubes, followed by a fast EET to (9,7) nanotubes and emission of the latter—under the assumption of negligible perturbation of $E_{11}$ energies in the aggregates. Our PL data for toluene-POF dispersions make this interpretation questionable. An increase in the "EET signals" correlated in Ref. 11 with a slow aggregation of nanotubes in a (metastable) aqueous dispersion could also be explained by the influence of aggregation and/or environment on the relative intensities of PL satellites. Indeed, we have already alluded to such dependence in the case of the $DE_1$ satellite. In addition, our recent PL+atomic force microscopy study of surface-deposited indi-

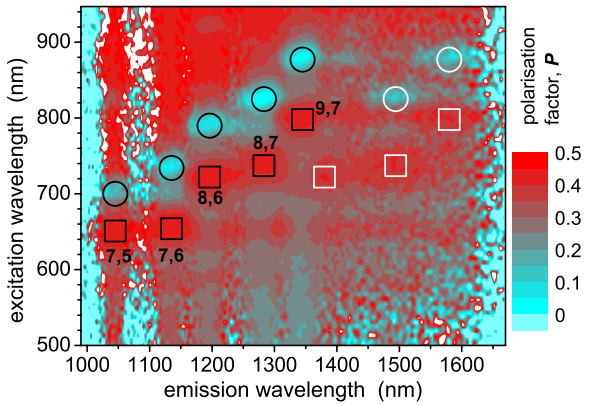


FIG. 5. (Color online) PL polarization factor vs emission and excitation wavelengths for HiPco nanotubes in toluene-POF (see Fig. 3). The main $E_{22}$-$E_{11}$ excitation-emission peaks of five emitting $(n,m)$ nanotubes and $DE_1$ emission satellites of (8,6), (8,7), and (9,7) nanotubes are marked with black and white open squares, respectively. Spots with a low polarization factor (open circles) correspond to transverse $E_{12,21}$ excitations (Ref. 9). White open circles indicate $DE_1$ emission satellites of (8,7) and (9,7) nanotubes excited via $E_{12,21}$ transitions.

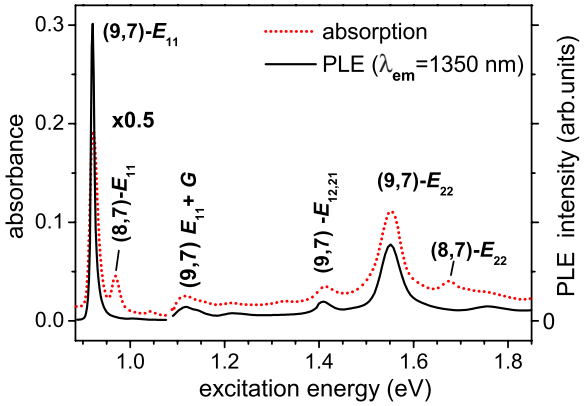


FIG. 6. (Color online) Absorption of PLV nanotubes in toluene-POF combined with a PLE spectrum ($\lambda_{emis}=1350$ nm) of the dominant (9,7) nanotubes. The PLE intensity is scaled to an equal area of (9,7)-$E_{11}$ peaks in the both spectra.

vidual and aggregated SWNTs has found dramatic broadening of the PL peaks caused by aggregation, but no unambiguous signatures of EET between "donor" and "acceptor" nanotubes.[24]

### C. Polarization measurements

Transverse $E_{12,21}$ photoexcitations can be particularly identified well in PL polarization maps (Fig. 5). They correspond to spots with a low polarization factor $P\sim0-0.05$ (marked with open circles). In contrast, the main $E_{22}$-$E_{11}$ peaks of all $(n,m)$ species in Fig. 5 (black open squares) exhibit $P\sim0.43$. These results are in a good agreement with a PL polarization study of SWNTs in an aqueous dispersion by Miyauchi *et al.*[10] Interestingly, the polarization map shown in Fig. 5 clearly reveals the $DE_1$ emission satellites excited via $E_{12,21}$ transitions (white open circles), which are hardly seen in the emission spectra. Note also that the low-$P$ spots at $E_{12,21}$ excitation and $E_{11}$ emission appear to consist of two components separated from each other by $\sim50-100$ meV along the excitation axis—as is particularly observed well for (7,6) and (8,7) nanotubes. The two components are presumably caused by a splitting between $E_{12}$ and $E_{21}$ excitations in SWNTs—similar to observations for SWNTs in an aqueous dispersion.[10]

A complementary polarization map for the $E_{11}$ excitation region is shown in Fig. S3 in Ref. 18. All PL features on this map, also including PL satellites discussed above, exhibit $P\sim0.4-0.5$ and are therefore related to axial optical excitations in SWNTs. The polarization of the main $E_{11}$-$E_{11}$ PL peaks ($P\sim0.45-0.5$) as well as their intensity (Fig. 3) provides evidence for a small contribution of the scattered (highly polarized) excitation light.

The values of $P$ measured in this and previous studies[10,25] for axial/transverse PL excitations in dispersed SWNTs are notably smaller/larger than the limiting values of +0.5/−0.33 for the ideal case of randomly oriented emitters with collinear/perpendicular absorption and emission transition moments.[14] One reason could be the high (up to hundreds of nanometers) diffusivity of excitons along SWNTs.[26] This would result in "loss" of the PL polarization if exciton generation and recombination sites had sufficiently different local orientations—which is not unreasonable given that individual nanotubes in dispersion have quite flexible configurations. For the transverse $E_{12,21}$ excitations, an additional "averaging" of $P$ is trivially caused by their partial overlap with the strong axial $E_{22}$ excitations (Figs. 2 and 3).

### D. Decay of the $E_{22}$ state: Pathways and efficiencies

Near-infrared emission of SWNTs has typically been measured in the "fingerprint" $E_{22}$ excitation region, providing structural assignment of luminescent species.[4] This already implies a substantial decay of the $E_{22}$ state to the emitting $E_{11}$ state. A comparison between absorption and PLE spectra of specific $(n,m)$ nanotubes (Figs. 1–3 and Fig. S2 in Ref. 18) allows us to quantitatively estimate a relative efficiency $\gamma$ for the $E_{22}\rightarrow E_{11}$ relaxation pathway according to

$$\gamma=\left[\int E_{22}(\mathrm{PLE})/\int E_{11}(\mathrm{PLE})\right]\times\left[\int E_{11}(\mathrm{abs})/\int E_{22}(\mathrm{abs})\right],\quad(0\le\gamma\le1),\quad(2)$$

where $\int E_{11,22}(\mathrm{PLE})$ and $\int E_{11,22}(\mathrm{abs})$ are the areas of the PLE and absorption peaks (approximated by Lorentzians). Clearly, of the samples studied here, the most precise estimate of $\gamma$ can be obtained for the nearly homogeneous dispersion of (9,7) nanotubes prepared from PLV material. Figure 6 combines the corresponding absorption and PLE spectra scaled to the same $E_{11}$ peak area in both spectra. The absorption curve follows the PLE spectrum with the exception of small peaks generated by (8,7) nanotubes. A somewhat higher background in the absorption spectrum can be attributed to residual metallic nanotubes and nanotube aggregates (which do not contribute to the PLE spectrum).

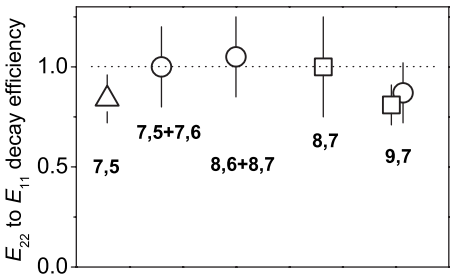


FIG. 7. Efficiency of $E_{22} \rightarrow E_{11}$ decay estimated for $(n,m)$ nanotubes in toluene-POF. Open squares, circles, and a triangle correspond to HiPco, PLV, and CoMo-CVD samples, respectively, and are plotted in order of increasing nanotube diameter. Mean values were estimated for (7,5) and (7,6) as well as for (8,6) and (8,7) nanotubes in HiPco dispersion because of their overlapping $E_{22}$ absorption bands (see Fig. 1).

According to Eq. (2), we determine the efficiency of $E_{22} \rightarrow E_{11}$ relaxation in (9,7) nanotubes to be $\gamma = 0.81 \pm 0.10$. A similar value was also obtained by averaging the $\int E_{22}$(PLE) and $\int E_{11}$(PLE) contributions across the emission profile of (9,7) nanotubes around $\lambda_{em} = 1350$ nm. Decay to the bright $E_{11}$ exciton is thus dominant for the bright $E_{22}$ exciton. The values of $\gamma$ evaluated for other $(n,m)$ species are plotted together in Fig. 7 in order of increasing nanotube diameter. These also include (7,5) nanotubes ($\gamma = 0.84 \pm 0.13$) constituting the major fraction in a toluene-POF dispersion of CoMo-CVD material. The absorption and PLE spectra of this sample are presented in Fig. S4 in Ref. 18. The estimated error margins in Fig. 7 mostly derive from background subtraction in the absorption spectra and from corrections of the PLE peaks for wavelength-dependent excitation intensity and Rayleigh scattering ($E_{11}$ peaks). The $E_{22}$ absorption of (7,5) and (7,6) as well as (8,6) and (8,7) nanotubes is strongly overlapping (Fig. 1). Therefore, we summed up the corresponding absorption and PLE peaks to calculate a mean value of $\gamma$ for these $(n,m)$ pairs in the HiPco dispersion. According to Fig. 7, the efficiency of $E_{22} \rightarrow E_{11}$ decay in the large-helical-angle $(n,m)$ species studied here is similarly high ($\gamma \geq 0.8$).

In view of the great variety of possible relaxation pathways via excitonic and continuum states around and below $E_{22}$, also including dark excitonic states below $E_{22}$ and $E_{11}$,[7–9,27] such efficient coupling between $E_{22}$ and $E_{11}$ optical excitons is puzzling. The same holds true for transverse $E_{12,21}$ excitations[28] and higher-energy $E_{33}$ and $E_{44}$ optical excitations, which also lead to the PL, i.e., relax to the $E_{11}$ bright exciton.[13] The recent study of Hertel *et al.*[6] provided a partial explanation in that decay of the $E_{22}$ exciton via electron-hole continuum states was inferred to be inefficient.[6] On the other hand, the corresponding calculations favored a phonon-assisted decay of the $E_{22}$ exciton to a dark state in the $E_{11}$ manifold of excitonic states. It is not clear why the latter state would then convert with a high yield to the bright $E_{11}$ exciton. Also note that the latter calculations made use of the zone-folding approximation that may oversimplify the excitonic structure in SWNTs.[5,7,8]

Our experimental data suggest that some decay of $E_{22}$ bright excitons into low-lying dark excitonic states does, in fact, occur. However, this is a minor pathway with efficiency limited to $\leq (1-\gamma) \sim 0.2$. This conclusion derives from a comparison of intensities of the $DE_{1,2}$ emission satellites upon $E_{22}$ vs $E_{11}$ excitations. When normalized to the $E_{11}$ emission peak areas, the $DE_{1,2}$ signals are a factor of $\sim 2-3$ higher upon $E_{22}$ excitation (see Fig. 2 and Fig. S2 in Ref. 18). This suggests an additional relaxation pathway $E_{22} \rightarrow DE_{1,2}$, without the intermediacy of an $E_{11}$ optical exciton. Because of the large energy separation between $E_{22}$ and $DE_{1,2}$, this relaxation pathway likely follows a staircase of dark excitonic states below $E_{22}$.

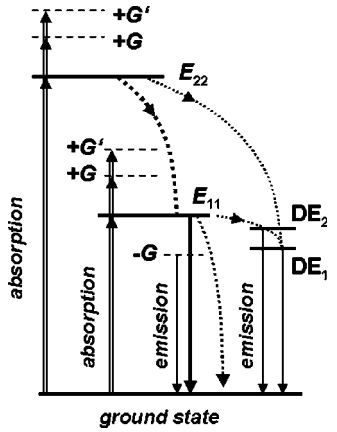


FIG. 8. Schematic diagram of experimentally observed one-photon optical absorption (doubled solid lines) and emission (single solid lines) transitions in semiconducting SWNTs. Phonon-coupled excitation and emission transitions are lettered with $+G$, $+G'$, and $-G$, respectively. Transverse $E_{12,21}$ excitations and PLE satellites $S$ (see text) are omitted. Dotted lines indicate possible relaxation pathways, including minor ones that couple the optical $E_{22}$ and $E_{11}$ excitonic states to proposed dark (weakly emitting) $DE_2$ and $DE_1$ states. Radiative recombination of the $E_{11}$ exciton is relatively effective ($\varphi_{PL} \sim 1.1\%$ in toluene-POF). The other emission transitions shown here are very weak by comparison.

A highly efficient $E_{22} \rightarrow E_{11}$ decay together with an approximately twofold to threefold increase in the $DE_{1,2}$ signals at $E_{22}$ vs $E_{11}$ excitation would imply that the $E_{11} \rightarrow DE_{1,2}$ relaxation pathway is not the only and, perhaps, not even the major decay channel for the $E_{11}$ optical exciton. Competing relaxation pathway(s) may involve other dark states predicted below $E_{11}$.[7,8,27] A schematic diagram of experimentally observed one-photon optical transitions, including PL excitation and emission satellites identified in this work, and the suggested relaxation pathways are presented in Fig. 8.

### E. Photoluminescence quantum yield

We have determined the PL quantum yield for (9,7) nanotubes dispersed in toluene-POF and excited into the $E_{22}$ state ($\lambda_{exc} = 800$ nm) to be $\varphi_{PL}(E_{22}) = (9 \pm 2) \times 10^{-3}$. This value is referred to the (9,7)-$E_{22}$ absorption peak with subtracted background. Taking into account the efficiency of $E_{22} \rightarrow E_{11}$ decay, we obtain $\varphi_{PL} \sim 1.1 \times 10^{-2}$ at $E_{11}$ excitation ($\lambda_{exc} = 1350$ nm). In analogy to other photophysical properties discussed above, very similar values of $\varphi_{PL}(E_{22})$ were also

found for (7,5), (7,6), (8,6), and (8,7) nanotubes (see Table S2 in Ref. 18). Values of $\varphi_{PL}(E_{22})$ around 1% are in a good agreement with the results of Nish *et al.*[1] and significantly larger than $\varphi_{PL}(E_{22}) \sim 0.1\%$ estimated for SWNTs in water-surfactant dispersions.[4,13] In this respect, toluene-POF seems to provide a less perturbing environment for SWNTs, approaching that of freely suspended SWNTs. For the latter, $\varphi_{PL}(E_{22})$ may approach a few percent.[29]

Recently, Tsyboulski *et al.*[30] measured the products of the absorption cross section (per mol of carbon) and PL quantum yield at $E_{22}$ excitation, $\varepsilon(E_{22}) \times \varphi_{PL}(E_{22})$, for individual nanotubes in a water-surfactant dispersion. For our set of $(n,m)$ species, they found an approximately twofold decrease in $\varepsilon(E_{22}) \times \varphi_{PL}(E_{22})$ by increasing the nanotube diameter (Table S2 in Ref. 18). If we assume approximately the same PL quantum yield for these species in aqueous dispersion (by analogy to SWNTs in toluene-POF), the above decrease in $\varepsilon(E_{22}) \times \varphi_{PL}(E_{22})$ implies that the absorption cross section (per mol of carbon) approximately doubles upon decreasing the nanotube diameter from 1.1 to 0.83 nm [corresponding to (9,7) and (7,5) nanotubes, respectively]. We caution that this correlation is probably limited to only large-helical-angle nanotubes. This can be proved as soon as additional $(n,m)$-narrowed dispersions or, even better, monodispersions of other $(n,m)$ species become available.

## IV. SUMMARY

We have shown that narrow $(n,m)$ distributions of semiconducting (7,5), (7,6), (8,6), (8,7), and (9,7) nanotubes can be obtained in toluene-POF dispersions. A near monodispersion was prepared for (9,7) nanotubes. The content of metallic species and residual nanotube aggregates appears to be strongly reduced in toluene-POF as compared to typical aqueous dispersions of SWNTs (see also Refs. 1 and 2). Moreover, SWNTs in toluene-POF demonstrate a relatively high PL quantum yield ($\sim 1\%$) and small emission linewidths ($\sim 17-19$ meV under $E_{22}$ excitation). These factors will prove very useful for many spectroscopic experiments on dispersed nanotubes. In this work, for instance, a number of fundamental photophysical parameters such as the efficiency of $E_{22} \rightarrow E_{11}$ decay and PL quantum yield could be accurately determined for specific $(n,m)$ nanotubes. Apart from low-intensity PL features already described in the literature, such as transverse $E_{12,21}$ excitation,[10] $G$- and $G'$-phonon-coupled PLE satellites,[20–23] and $DE_{1,2}$ emission satellites,[8,9] the enhanced-quality PL maps obtained for toluene-POF dispersions revealed a further PLE satellite at $\sim(E_{11}+95)$ meV and $G$-phonon-coupled *emission* satellite at $\sim(E_{11}-200)$ meV.

The $(n,m)$ nanotubes studied here surprisingly demonstrate similar behavior with regard to the efficiency of $E_{22} \rightarrow E_{11}$ relaxation ($\gamma \geq 0.8$), PL quantum yield, and PL peak patterns. This is likely due to their close-lying structures both in terms of the helical angle and diameter. Photophysically relevant electronic (excitonic) states and relaxation processes are apparently quite similar in these nanotubes. This is likely to be the case not only in toluene-POF but also in other environments. However, absolute relaxation rates and efficiencies (e.g., PL quantum yield) are, of course, strongly matrix dependent.

According to our estimates [most precise for (7,5) and (9,7) nanotubes], the efficiency of $E_{22} \rightarrow E_{11}$ decay is high but less than unity. This indicates the existence of additional, minor relaxation pathways for the optical $E_{22}$ exciton, without the intermediacy of the optical $E_{11}$ exciton. These likely involve dark excitonic states as suggested by increase in weak $DE_{1,2}$ emission under $E_{22}$ vs $E_{11}$ photoexcitation.

A superposition of numerous PL excitation and emission satellites of several $(n,m)$ species in the $E_{11}$ excitation region produces characteristic crossed stripes patterns in two-dimensional PL maps. An analogous pattern for SWNTs in a water-surfactant dispersion (although with broader PL features) has recently been interpreted as a signature of energy transfer between different $(n,m)$ species in nanotube aggregates.[11] PL maps of SWNTs in toluene-POF—in a dispersion nearly free from nanotube aggregates—draw this interpretation into question.

A present "disadvantage" of the $(n,m)$-narrowed dispersions prepared in this work is their limitation to only a few $(n,m)$ nanotubes with large helical angles. Consequently, optical properties could be determined only for these, closely related structures. We believe, however, that this limitation may be overcome in view of the great potential for chemical modification and adjustment of polymer and/or organic solvent systems to specific $(n,m)$ nanotubes.

## ACKNOWLEDGMENTS

This work was supported in part by the Deutsche Forschungsgemeinschaft (DFG) and by the Bundesministerium für Bildung und Forschung (BMBF).

*Corresponding authors.
†lebedkin@int.fzk.de
‡manfred.kappes@chemie.uni-karlsruhe.de

[1] A. Nish, J.-Y. Hwang, J. Doig, and R. J. Nicholas, Nat. Nanotechnol. **2**, 640 (2007).
[2] F. Chen, B. Wang, Y. Chen, and L.-J. Li, Nano Lett. **7**, 3013 (2007).
[3] S. Giordani, S. D. Bergin, V. Nicolosi, S. Lebedkin, M. M. Kappes, W. J. Blau, and J. N. Coleman, J. Phys. Chem. B **110**, 15708 (2006).
[4] M. J. O'Connell, S. M. Bachilo, C. B. Huffman, V. C. Moore, M. S. Strano, E. H. Haroz, K. L. Rialon, P. J. Boul, W. H. Noon, C. Kittrell, J. Ma, R. H. Hauge, R. B. Weisman, and R. E. Smalley, Science **297**, 593 (2002).
[5] M. S. Dresselhaus, G. Dresselhaus, R. Saito, and A. Jorio, Annu. Rev. Phys. Chem. **58**, 719 (2007).
[6] T. Hertel, V. Perebeinos, J. Crochet, K. Arnold, M. Kappes, and P. Avouris, Nano Lett. **8**, 87 (2008).

[7] H. Zhao and S. Mazumdar, Phys. Rev. Lett. **93**, 157402 (2004).
[8] G. D. Scholes, S. Tretiak, T. J. McDonald, W. K. Metzger, C. Engtrakul, G. Rumbles, and M. J. Heben, J. Phys. Chem. C **111**, 11139 (2007).
[9] O. Kiowski, K. Arnold, S. Lebedkin, F. Hennrich, and M. M. Kappes, Phys. Rev. Lett. **99**, 237402 (2007).
[10] Y. Miyauchi, M. Oba, and S. Maruyama, Phys. Rev. B **74**, 205440 (2006).
[11] P. H. Tan, A. G. Rozhin, T. Hasan, P. Hu, V. Scardaci, W. I. Milne, and A. C. Ferrari, Phys. Rev. Lett. **99**, 137402 (2007).
[12] F. Hennrich, R. Krupke, S. Lebedkin, K. Arnold, R. Fischer, and M. M. Kappes, J. Phys. Chem. B **109**, 10567 (2005).
[13] S. Lebedkin, K. Arnold, F. Hennrich, R. Krupke, B. Renker, and M. M. Kappes, New J. Phys. **5**, 140 (2003).
[14] J. R. Lakowicz, *Principles of Fluorescence Spectroscopy* (Plenum, New York, 1999).
[15] S. Lebedkin, T. Langetepe, P. Sevillano, D. Fenske, and M. M. Kappes, J. Phys. Chem. B **106**, 9019 (2002).
[16] R. B. Weisman and S. M. Bachilo, Nano Lett. **3**, 1235 (2003).
[17] O. Kiowski, S. Lebedkin, F. Hennrich, S. Malik, H. Rösner, K. Arnold, C. Sürgers, and M. M. Kappes, Phys. Rev. B **75**, 075421 (2007).
[18] See EPAPS Document No. E-PRBMDO-77-091816 for (Fig. S1) PL map of PLV nanotubes dispersed in toluene-POF without ultracentrifugation; (Fig. S2) PLE spectra of five $(n,m)$ species in the dispersion of HiPco SWNTs; (Fig. S3) PL polarization map in the $E_{11}$ excitation region; (Fig. S4) absorption vs PLE spectra of (7,5) nanotubes in the dispersion of CoMo-CVD nanotubes; (Table S1) PL peak energies and assignments and (Table S2) PL quantum yields for $(n,m)$ nanotube in toluene-POF. For more information on EPAPS, see http://www.aip.org/pubservs/epaps.html.
[19] R. Saito, G. Dresselhaus, and M. S. Dresselhaus, *Physical Properties of Carbon Nanotubes* (Imperial College, London, 1998).
[20] F. Plentz, H. B. Ribeiro, A. Jorio, M. S. Strano, and M. A. Pimenta, Phys. Rev. Lett. **95**, 247401 (2005).
[21] Y. Miyauchi and S. Maruyama, Phys. Rev. B **74**, 035415 (2006).
[22] H. Htoon, M. J. O'Connell, S. K. Doorn, and V. I. Klimov, Phys. Rev. Lett. **94**, 127403 (2005).
[23] J. Lefebvre and P. Finnie, Phys. Rev. Lett. **98**, 167406 (2007).
[24] S.-S. Jester, O. Kiowski, S. Lebedkin, F. Hennrich, R. Fischer, N. Stürzl, J. Hawecker, and M. M. Kappes, Phys. Status Solidi B **244**, 3973 (2007) b.
[25] S. Lebedkin, F. Hennrich, T. Skipa, and M. M. Kappes, J. Phys. Chem. B **107**, 1949 (2003).
[26] C.-X. Sheng, Z. V. Vardeny, A. B. Dalton, and R. H. Baughman, Phys. Rev. B **71**, 125427 (2005).
[27] S. Tretiak, Nano Lett. **7**, 2201 (2007).
[28] We estimated the efficiency of $E_{12,21} \rightarrow E_{11}$ relaxation in (9,7) nanotubes in toluene-POF to be $\geq 0.7$.
[29] J. Lefebvre, D. G. Austing, J. Bond, and P. Finnie, Nano Lett. **6**, 1603 (2006).
[30] D. A. Tsyboulski, J.-D. R. Rocha, S. M. Bachilo, L. Cognet, and R. B. Weisman, Nano Lett. **7**, 3080 (2007).